Coupled transport in rotor models

2016 New J. Phys. 18 083023

(http://iopscience.iop.org/1367-2630/18/8/083023)

New Journal of Physics
The open access journal at the forefront of physics

Deutsche Physikalische Gesellschaft DPG
IOP Institute of Physics

Published in partnership with: Deutsche Physikalische Gesellschaft and the Institute of Physics

OPEN ACCESS

RECEIVED
23 March 2016

REVISED
1 July 2016

ACCEPTED FOR PUBLICATION
11 July 2016

PUBLISHED
3 August 2016

PAPER

Coupled transport in rotor models

S Iubini[1,7], **S Lepri**[2,3], **R Livi**[2,3,4,5] **and A Politi**[6]

[1] Centre de Biophysique Moléculaire (CBM), CNRS-UPR 4301 Rue Charles Sadron, F-45071 Orléans, France
[2] Consiglio Nazionale delle Ricerche, Istituto dei Sistemi Complessi, via Madonna del Piano 10, I-50019 Sesto Fiorentino, Italy
[3] Istituto Nazionale di Fisica Nucleare, Sezione di Firenze, via G. Sansone 1 I-50019, Sesto Fiorentino, Italy
[4] Dipartimento di Fisica e Astronomia, Università di Firenze, via G. Sansone 1 I-50019, Sesto Fiorentino, Italy
[5] Centro Interdipartimentale per lo Studio delle Dinamiche Complesse, Università di Firenze, Italy
[6] Institute for Complex Systems and Mathematical Biology & SUPA University of Aberdeen, Aberdeen AB24 3UE, UK
[7] Author to whom any correspondence should be addressed.

E-mail: stefano.iubini@cnrs-orleans.fr, stefano.lepri@isc.cnr.it, roberto.livi@unifi.it **and** a.politi@abdn.ac.uk

Keywords: transport processes, heat transfer (theory), nonlinear oscillators, XY model, discrete nonlinear Schrdinger equation

Abstract

Steady nonequilibrium states are investigated in a one-dimensional setup in the presence of two thermodynamic currents. Two paradigmatic nonlinear oscillators models are investigated: an XY chain and the discrete nonlinear Schrödinger equation. Their distinctive feature is that the relevant variable is an angle in both cases. We point out the importance of clearly distinguishing between energy and heat flux. In fact, even in the presence of a vanishing Seebeck coefficient, a coupling between (angular) momentum and energy arises, mediated by the unavoidable presence of a *coherent* energy flux. Such a contribution is the result of the 'advection' induced by the position-dependent angular velocity. As a result, in the XY model, the knowledge of the two diagonal elements of the Onsager matrix suffices to reconstruct its transport properties. The analysis of the nonequilibrium steady states finally allows to strengthen the connection between the two models.

1. Introduction

The physics of open (classical or quantum) many-particle systems is a vast interdisciplinary field ranging from the more basic theoretical foundations to the development of novel technological principles for energy and information management. Within this broad context, simple models of classical nonlinear oscillators have been investigated to gain a deeper understanding of heat transfer processes far from equilibrium [1–3] (see also [4] for a recent account). The existing literature mostly focused on the case where just one quantity, the energy, is exchanged with external reservoirs and transported across the system—see e.g. [5–9] for some recent work. In general, however, the dynamics of physical systems is characterized by more than one conserved quantity each associated with a hydrodynamic mode of spontaneous fluctuations [10–12]. Under the action of external reservoirs, one expects the corresponding currents to be coupled in the usual sense of linear irreversible thermodynamics. A well-known example is that of thermoelectric phenomena whereby useful electric work can be extracted in the presence of temperature gradients.

From the point of view of statistical mechanics, a few works have been so far devoted to coupled transport: they can be grouped in those devoted to interacting particle gases [13–15] and to coupled oscillator systems [16–20]. The connection between microscopic interactions and macroscopic thermodynamic properties is still largely unexplored. In this paper, we provide a detailed characterization of coupled transport in possibly the simplest dynamical model, the one-dimensional rotor model, also termed Hamiltonian XY model [21]. Here, there are two conserved quantities (energy and angular momentum), two associate currents, and only one relevant thermodynamic parameter, the temperature.

The simplicity of the model reveals the crucial role played by the *coherent* energy flux, normally present in steady nonequilibrium states: it represents the part of the energy current advected by the local average angular momentum. In a sense, it is the mediator in the coupling between the two currents. As a result, it is absolutely

necessary to distinguish between energy and heat fluxes, as only the former one takes fully into account the coherent contribution.

Previous studies of the Hamiltonian XY model (referred to in the following as XY model for brevity) essentially focused on the transport of heat, in the absence of an angular-momentum flux. In such a setup, the model is an example where transport is normal in 1D in spite of the momentum being conserved [22–25]. There are two complementary views to account for this behavior. In the general perspective of nonlinear fluctuating hydrodynamics [10, 26] normal diffusion can be explained by observing that the angle variables do not constitute a conserved field, which leads to the absence of long-wavelength currents in the system [27]. From a dynamical point of view, one can invoke that normal transport sets in due to the spontaneous formation of local excitations, termed rotobreathers, that act as scattering centers [28]. Phase slips (jumps over the energy barrier), on their side, may effectively act as localized random kicks, that contribute to scatter the low-frequency modes, thus leading to a finite conductivity. Actually, such long-lived localized structures lead also to anomalously slow relaxation to equilibrium [29, 30]. Non stationary (time dependent) heat exchange processes have also been shown to be peculiar [31]. The effect of external forces has been previously addressed only in [32] and boundary-induced transitions have also been discovered [33] (see also [34]). The important extension to 2D is characterized by the presence of a Kosterlitz–Thouless–Berezinskii phase transition between a disordered high-temperature phase and a low-temperature one, displaying anomalous and normal transport respectively [35].

More recently, the 1D XY model has attracted the interest in a different context for some nontrivial properties related to the transport of angular momentum or, using a different language, electric charge [36]. In fact, it can be also interpreted as the classical limit of an array of Josephson junctions. In the quantum version, a many body localization phenomenon, associated to an ergodicity breaking mechanism, has been observed and proved to exist. In the classical limit, the frequency can be interpreted as a charge variable, so that the transport of charge is nothing but the current of angular momentum in the standard representation.

In section 2 we review the general thermodynamic formalism of linear-response and then develop specific relationships for the XY model that are later used to interpret the results of numerical simulations.

A careful analysis of nonequilibrium stationary states in coupled transport requires an appropriate definition of the reservoirs controlling two fluxes at the same time. This point is discussed in section 3, where we provide a comparison between a Langevin and a collisional stochastic scheme.

The results of numerical simulations of coupled transport in the XY model are presented in section 4, where we also describe how to determine the dependence of the Onsager coefficients on the temperature, when a suitable reference frame for the frequencies is adopted. The numerical analysis confirms the prediction of linear Onsager theory, according to which the Onsager coefficients of the XY model do not depend on the frequency and that no coupled transport is present in the heat-representation.

In order to test to what extent the scenario reconstructed for the XY model applies to more general models, where thermodynamic properties depend also on the chemical potential, we study the discrete nonlinear Schrödinger (DNLS) model and compare its nonequilibrium behavior with that of a 1D XY chain. It was recently argued that the high mass-density regime of the DNLS equation can be mapped onto an XY chain [37]. In section 5 we reconsider the mapping between these two models in the framework investigating the corresponding Onsager coefficients. As a result, we confirm the existence of a zero-Seebeck coefficient line, whose very existence can be used as a reference to quantify the deviations from the XY dynamics. Conclusions and perspectives are discussed in section 6.

2. Theoretical framework and the rotor chain model

A great deal of the recent literature on transport phenomena in one-dimensional systems is focused on heat transport alone [1, 2]. In such cases, the relevant physical observables are the heat flux j_q and the corresponding thermodynamic force, namely the gradient of temperature T (in what follows we equivalently refer to T or $\beta = 1/T$, selecting the more appropriate quantity for the theoretical description). They are related by the Fourier equation

$$j_q = -\kappa \frac{\mathrm{d}T}{\mathrm{d}y},$$

where κ is the heat conductivity, and y is the spatial direction of the applied gradient. The variable y represents the spatial position along the chain (without prejudice of generality its length can be normalized to unit, i.e. $0 \leqslant y \leqslant 1$)

In this section we describe the formalism of coupled transport in one-dimensional systems where a second quantity is transported: we call it 'momentum', but it could be any other physical observable like mass, charge, etc (a related discussion for particle models is given for instance in [14]).

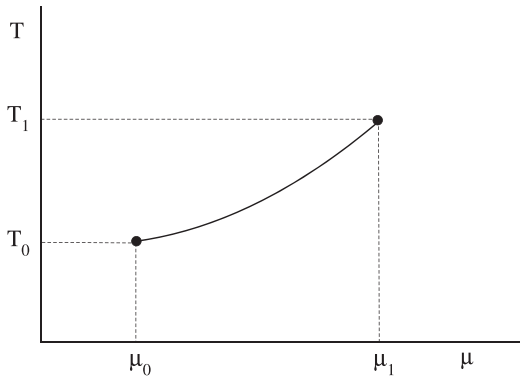

Figure 1. Schematic view of the local equilibrium state of a chain in contact with two heat baths at temperature T_0, T_1 and chemical potential μ_0, μ_1.

Its flux is denoted by j_p and the corresponding thermodynamic force is the gradient of chemical potential μ. Within linear nonequilibrium thermodynamics, coupled transport can be characterized by making use of two equivalent representations. The heat-representation can be viewed as the extension of the pure heat transport process, since it takes into account the equations for momentum and heat fluxes:

$$\begin{aligned} j_p &= -L_{pp}\beta\frac{\mathrm{d}\mu}{\mathrm{d}y} + L_{pq}\frac{\mathrm{d}\beta}{\mathrm{d}y}, \\ j_q &= -L_{qp}\beta\frac{\mathrm{d}\mu}{\mathrm{d}y} + L_{qq}\frac{\mathrm{d}\beta}{\mathrm{d}y}. \end{aligned} \tag{1}$$

where L_{xx} are the entries of the symmetric Onsager matrix (for pure heat transport the only nonzero entry is $L_{qq} = \kappa\ \beta^2$). In coupled transport phenomena, these quantities play the role of generalized transport coefficients and, usually, they are expected to depend on β and μ.

In the energy–representation, rather than referring to j_q, the energy flux j_h is considered, whose corresponding thermodynamic force is the gradient of $\mu\beta$. The coupled transport equations read

$$\begin{aligned} j_p &= -L'_{pp}\frac{\mathrm{d}\beta\mu}{\mathrm{d}y} + L'_{ph}\frac{\mathrm{d}\beta}{\mathrm{d}y} \\ j_h &= -L'_{hp}\frac{\mathrm{d}\beta\mu}{\mathrm{d}y} + L'_{hh}\frac{\mathrm{d}\beta}{\mathrm{d}y}\ , \end{aligned} \tag{2}$$

where L'_{xx} is a new symmetric Onsager matrix, whose entries depend in general on β and μ. In both representations the validity of the set of the linear response equations is conditioned to the existence of local thermodynamic equilibrium.

As a suitable model for coupled transport in one dimension we consider a chain of particles, whose left ($y = 0$) and right ($y = 1$) boundaries are in contact with two reservoirs, operating at different temperatures, T_0 and T_1, and chemical potentials, μ_0 and μ_1. Within the ($\mu,\ T$)-plane, the variation of these thermodynamic variables along the chain can be represented as a path starting from an 'initial' state ($\mu_0,\ T_0$) and ending in the 'final' one ($\mu_1,\ T_1$), or vice versa (see figure 1). This task can be naturally accomplished in the energy-representation. In fact, when a stationary regime is established, j_p and j_h have to be constant along the chain. Accordingly, the shape of the path shown in figure 1 is obtained by integrating the set of differential equations (2). There are two important remarks about the integration procedure: (i) it can be performed explicitly if the dependence of the corresponding Onsager matrix elements L'_{xx} on $\beta\,(T)$ and μ is known; (ii) the set of differential equations have to fulfill four boundary conditions, that fix the values of the two temperatures and of the two chemical potentials imposed by the reservoirs. These four conditions suffice to determine the values of the two fluxes and of the two integration constants.

Notice that when stationary conditions for coupled transport are established, j_q, at variance with j_h, is not constant along the chain and the path reconstruction in ($\mu,\ T$)-plane in the heat-representation is more involved. This notwithstanding, the set of equations (1) reveals useful for studying coupled transport in models like the XY chain. This is a model of nearest-neighbor coupled rotors, whose interaction energy depends on a phase variable ϕ. The equations of motion read

$$I\ddot{\phi}_i = U\,[\,\sin(\phi_{i+1} - \phi_i) - \sin(\phi_i - \phi_{i-1})], \tag{3}$$

where I is the moment of inertia of the rotors, U is the amplitude of the potential energy barrier and the integer i labels the sites along the chain ($y = i/N$ and $i = 0, \cdots, N$). The associated Hamiltonian function is

$$H = \sum_i \frac{\lambda_i^2}{2I} + U[1 - \cos(\phi_{i+1} - \phi_i)], \tag{4}$$

where $\lambda_i = I\dot{\phi}_i$ denotes the angular momentum of site i. The total angular momentum $\Lambda = \sum_i \lambda_i$ and the total energy H are conserved quantities of the XY dynamics, equation (3).

Passing to thermodynamics, the microscopic expressions for momentum and heat fluxes of the model are

$$j_p(i) = -U\langle \sin(\phi_{i+1} - \phi_i)\rangle, \quad j_q(i) = -U\langle (\dot{\phi}_i - \langle\dot{\phi}_i\rangle)\sin(\phi_{i+1} - \phi_i)\rangle, \tag{5}$$

where the average $\langle\cdot\rangle$ is over stationary conditions yielding local thermodynamic equilibrium. The chemical potential μ coincides with the rotation frequency ω of the rotors. The term proportional to $\langle\dot{\phi}_i\rangle$ is precisely what we referred to above as the coherent part of the flux.

The dependence of the interaction term in the equation of motion (3) on a trigonometric function of the phase variables induces quite peculiar features of coupled transport. First of all, in the heat representation the off-diagonal terms $L_{qp} = L_{pq}$ vanish: the heat current cannot induce a momentum current in a system which, on average, does not rotate. Mathematically, this follows from the opposite parity of energy and momentum currents under time reversal symmetry, so that the Green–Kubo formula gives vanishing Onsager cross terms [38]. Therefore, equation (1) simplifies to

$$\begin{aligned} j_p &= -L_{pp}\beta\frac{\mathrm{d}\omega}{\mathrm{d}y}, \\ j_q &= L_{qq}\frac{\mathrm{d}\beta}{\mathrm{d}y}. \end{aligned} \tag{6}$$

Moreover, L_{pp} and L_{qq} cannot depend on ω. In fact, given any local oscillation frequency ω, one can always choose a suitable rotating frame where $\omega = 0$. Since the physical properties of coupled transport must be independent on the choice of the reference frame, L_{pp} and L_{qq} should depend on T only. At the first glance, these arguments seem to suggest that the underlying physics is pretty trivial, since it corresponds to two uncoupled transport processes in the heat-representation. However, passing to the energy-representation, where

$$j_h = j_q + \omega j_p, \tag{7}$$

simple calculations reveal that

$$L'_{pp} = L_{pp}, \quad L'_{ph} = L'_{hp} = L_{pp}\omega, \quad L'_{hh} = L_{qq} + \omega^2 L_{pp}.$$

Altogether, the matrix L' is symmetric (as it should) and, more importantly, its off-diagonal terms do not vanish. The relationship with the heat representation reveals that the three coefficients defining L' are not independent: all statistical properties of the XY model are captured by two quantities only: L_{pp} and L_{qq}.

In order to obtain a complete characterization of coupled heat transport of the XY model in the energy-representation one has to determine the actual value to be attributed to ω, since it depends on the rotating reference frame adopted for the entire system. Notice that this situation is analogous to the standard ambiguity of defining a potential up to a constant or of fixing a suitable gauge.

This problem can be solved by shifting the origin of the frequency axis in such a way that the energy flux vanishes. Once we have introduced

$$\omega_e = \omega - \overline{\omega}, \tag{8}$$

the condition $j_q + \omega_e j_p = 0$ (see equation (7)) implies

$$\overline{\omega} = j_h/j_p. \tag{9}$$

As long as $j_p \neq 0$, $\overline{\omega}$ is a well defined variable. Accordingly, we can 'fix the gauge' by measuring the frequency ω in the reference frame where the energy flux vanishes.

As a final step, we want to reconstruct the path described in the plane (ω, β), while moving along the chain. It can be obtained by dividing term by term the two equations in (6) and by recalling that $j_q = -\omega j_p$ (see equation (5)). One finds the simple equation

$$\frac{\mathrm{d}\beta}{\mathrm{d}\omega} = \frac{L_{pp}}{L_{qq}}\beta\omega, \tag{10}$$

where both L_{pp} and L_{qq} depend only on β. It is convenient to rewrite equation (10) in terms of the temperature T and the squared frequency $\sigma = \omega^2$

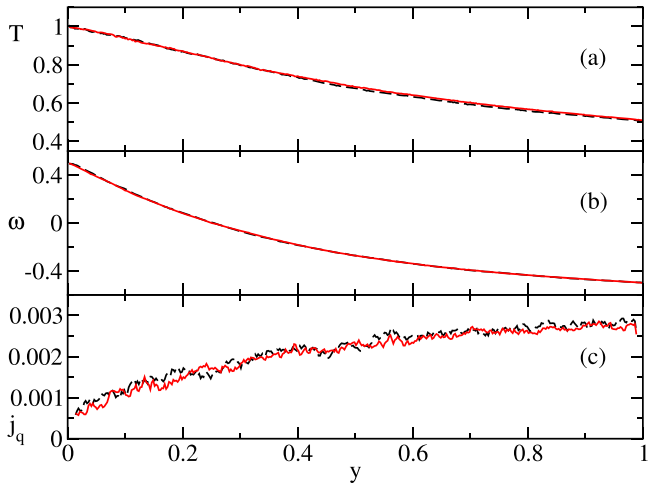

Figure 2. Stationary nonequilibrium profiles corresponding to the parameters $\omega_0 = 0.5$, $\omega_1 = -0.5$, $T_0 = 1$, $T_1 = 0.5$ in a chain with $N = 400$ particles. (a) Temperature profiles; (b) frequency (chemical potential) profiles; (c) local heat fluxes. Black dashed curves refer to Langevin heat baths with coupling parameter $\gamma = 1$, implemented within a 4th order Runge–Kutta integration scheme (time step 10^{-2}). Red curves are obtained using collisional heat baths with Poissonian distribution of collision times $\sim\exp(-\gamma_c t)$ and $\gamma_c = 1$, implemented within a 4th order MacLachlan–Atela (symplectic) integrator (time step 10^{-2} and total integration time 10^7).

$$\frac{\mathrm{d}T}{\mathrm{d}\sigma} = -\frac{L_{pp}}{L_{qq}}\frac{T}{2}. \tag{11}$$

The path in the $(\sigma,\ T)$-plane can be obtained by formally integrating the above equation

$$\sigma = \int_T^{T_{\max}} \mathrm{d}\tau \frac{L_{qq}}{L_{pp}}\frac{2}{\tau}, \tag{12}$$

where $T_{\max}$ is the maximum value reached by the temperature T along the chain (see section 4).

3. Thermal baths

Various schemes can be employed for modeling the heat exchange of a physical system with a reservoir. The two most widely used are: (i) Langevin heat baths; (ii) stochastic collisions [1, 2]. The former setup amounts to adding a pair of dissipating/fluctuating terms to the equations of motion of the boundary particles. In the latter one, the boundary particles are assumed to exchange their velocity with equal-mass particles from an external heat bath, in equilibrium at some given temperature T.

Both schemes can be easily generalized to account for an exchange of angular momentum, as well. In [33], the following Langevin scheme was proposed (here we just refer to the last particle)

$$I\ddot{\phi}_N = F(\phi_N - \phi_{N-1}) - F(\phi_{N+1} - \phi_N) + \gamma(\omega_1 - \dot{\phi}) + \sqrt{2\gamma T}\ \xi(t), \tag{13}$$

where the function F is the torque acting between nearest–neighbor particles and ω_1 can be interpreted as the frequency, or chemical potential, imposed by the stochastic bath via the external torque $\gamma\omega_1$, where γ defines the coupling strength with the bath. The quantity $\xi(t)$ accounts for a Gaussian white random noise with zero mean and unit variance, while the value of ϕ_{N+1} depends on the choice of boundary conditions: i.e. it is set equal to ϕ_N for open boundary conditions, or to 0 for fixed boundary conditions.

In the stochastic approach, the action of a reservoir imposing an average frequency ω_1 can be simulated by randomly resetting the velocity $\dot{\phi}_N$ of the end particle at random times (with some given average frequency), according to the distribution

$$P(\nu) = \sqrt{\frac{I}{\pi T}}\,\mathrm{e}^{-I(\nu-\omega_1)^2/T}.$$

In this scheme, the bath frequency ω_1 enters as a shift of the Gaussian distribution of ν [8].

Numerical tests reveal that these schemes are essentially equivalent to one another at finite temperature (see the simulation data reported in figure 2). However, this equivalence does not hold anymore in the limit case where temperature is set to 0. Indeed there is a difference in the two schemes: the collisional setup maintains

[8] It is worth mentioning that a different strategy has been adopted by the authors of [36], who have explored a case where no heat exchange is involved. They have assume directly $\phi_{N+1} = \omega_1 t$ (without any extra torque).

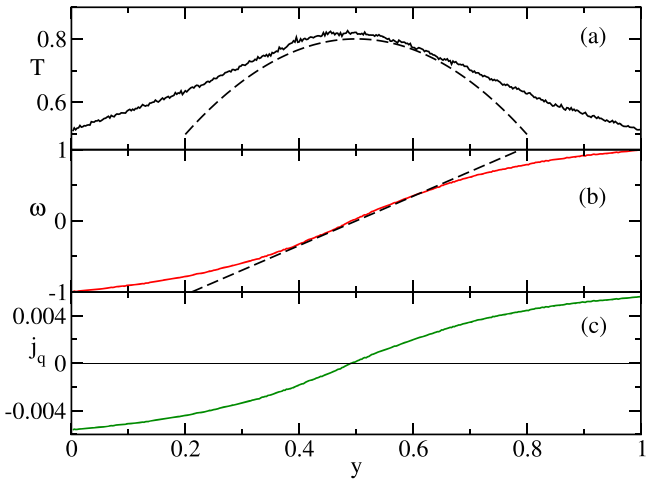

Figure 3. Some observables (solid lines) for an XY chain of 400 particles, in contact at its boundaries with two heat baths at temperature $T_0 = T_1 = 0.5$ and in the presence of torques $\omega_0 = -1$ and $\omega_1 = 1$: (a) temperature profile; (b) frequency (chemical potential) profile; (c) local heat flux. The dashed lines in panels (a) and (b) refer to the profiles derived in the limit of constant momentum conductivity, see the text at the end of the section.

some stochasticity due to the random times of the collisions, while the Langevin setup reduces to a purely deterministic (dissipative) dynamics. The interesting consequences emerging from such a difference will be investigated in a separate paper, devoted to a specific study of the limit case of zero-temperature heat baths.

4. Numerical simulations of coupled transport in the XY chain

We start this section by illustrating qualitatively how coupled transport manifests itself. In figure 3, we show the frequency and temperature profile in a case where both thermal baths are set to the same temperature and torques $\omega_0 = -1$ and $\omega_1 = 1$ are applied at the chain ends.

The temperature profile exhibits a bump in the middle of the chain (as first found in [32]). The variation of the temperature along the chain is a consequence of the coupling with the momentum flux imposed by the torque at the boundaries, although, in the end, the energy flux vanishes (for symmetry reasons). By recalling that $j_h = j_q + \omega j_p$ we see that the heat flux $j_q = -\omega j_p$ varies along the chain being everywhere proportional to the frequency, so that it is negative in the left part and positive in the right side (this is again consistent with symmetry considerations). In practice one can conclude that heat is generated in the central part, where the temperature is higher and transported towards the two edges. The total energy flux is however everywhere zero as the heat flux is compensated by an opposite coherent flux due to momentum transfer.

Altogether, the presence of the temperature bump can be interpreted as a sort of Joule effect: the transport of momentum involves a dissipation which in turn contributes to increasing the temperature, analogously to what happens when an electric wire is crossed by a flux of charges.

The nonlinear profiles of both frequency and temperature in figures 2 and 3 reflect the dependence of the transport coefficients on the temperature. The following thereotical analysis aims at clarifying how such a dependence can be extracted from numerical simulations. Afterwards, at the end of this section, we revisit the problem of the actual shape of such profiles.

The flux of momentum j_p is obviously constant along the chain. It can be used to determine the dependence of L_{pp} on T,

$$L_{pp} = -Tj_p \frac{\mathrm{d}y}{\mathrm{d}\omega}. \tag{14}$$

Since only the differential of ω is involved in this equation, there is no need to distinguish between ω and ω_e (see equation (8)).

The results of numerical simulations are plotted in figure 4: the black curves are obtained by simulating a long chain submitted to a relatively large temperature difference, while the squares correspond to small gradients. The good agreement confirms the assumption of a local thermal equilibrium. L_{pp} exhibits a divergence for decreasing values of T (notice that the vertical axis is logarithmic). This reflects the Arrhenius-type behavior of the thermal conductivity that has been previously demonstrated [22, 23]. In the temperature range explored in this paper, a power-law fit suggests that $L_{pp} \sim T^{-2.2}$. However, the suppression of momentum

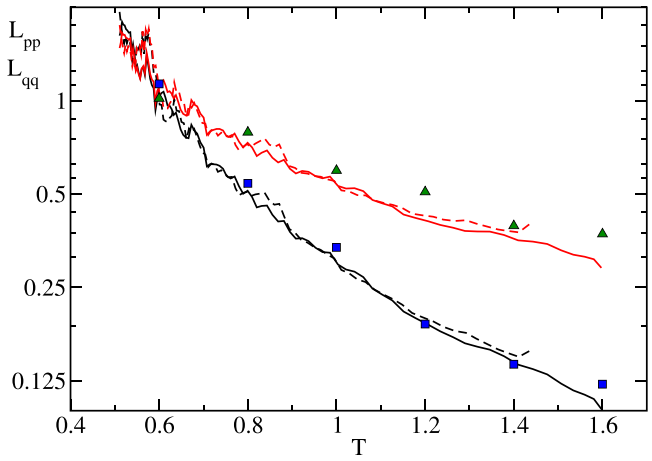

Figure 4. The two diagonal coefficients of the Onsager matrix obtained using equation (14) in simulations of a chain 800 sites long and Langevin dynamics equation (13). All curves correspond to $T_l = 0.5$. The solid curves have been obtained for $\omega_1 = 2$, while at $y = 0$ no thermal bath nor torque and fixed boundary conditions have been applied. The dashed lines correspond to $\omega_1 = 1.5$, $\omega_0 = 0$ and $T_0 = 1.5$. Black (lower) and red (upper) lines correspond to L_{pp} and L_{qq}, respectively. The symbols have been obtained by implementing the Langevin reservoirs, equation (13) to impose either small differences of temperature or chemical potential and thereby invoking equation (6). More precisely, L_{qq} (green triangles) was computed imposing a temperature gradient $\Delta T = T_l - T_0 = 2T/5$ and $\Delta\omega = \omega_1 - \omega_0 = 0$, while L_{pp} (blue squares) was obtained by setting $\Delta T = 0$ and $\Delta\omega = T/4$. Simulations refer to an XY chain with $N = 512$.

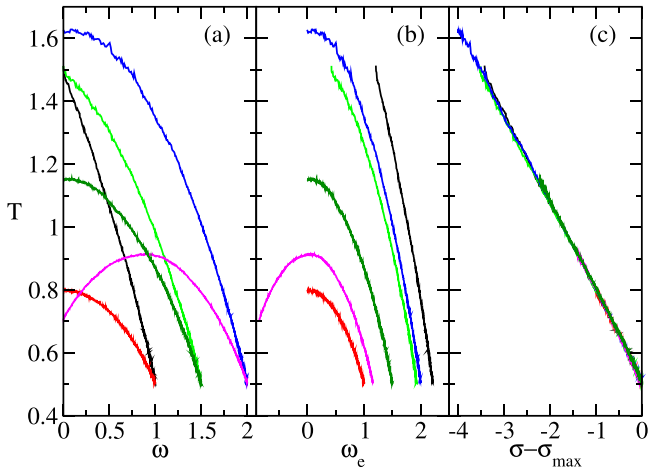

Figure 5. Different representations of various nonequilibrium paths. Panel (a) refers to the real frequency ω, observed in the numerical experiments; the frequency in panel (b) is shifted as in equation (8)), i.e. it corresponds to the frequency measured in the frame, where the energy current vanishes; panel (c) refers to the square square effective frequency $\sigma = \omega_e^2$, suitably shifted to let the curves start from the same point in the bottom right. All curves refer to an XY chain of 800 particles. In all simulations, fixed boundary conditions are assumed on the left boundary and a temperature $T_l = 0.5$ is fixed on the right. The red, dark green, and blue lines have been obtained with no heat bath on the left and $\omega_1 = 1$, 1.5, and 2, respectively. The purple line corresponds to $T_0 = 0.7$, $\omega_1 = 2$, the black line corresponds to $T_0 = 1.5$, $\omega_1 = 1$, the light green line corresponds to $T_0 = 1.5$, $\omega_1 = 1.5$.

transport in the high-temperature limit is much stronger. In a recent paper [36], an exponential decrease of momentum conductivity has been suggested as a result of an effective ergodicity breaking. In fact, it has been therein conjectured that, at high temperatures, the rotor chain enters a 'bad metal' conducting phase.

The red curves refer to L_{qq}: they have been obtained indirectly from the knowledge of the ratio L_{pp}/L_{qq}, determined by following the procedure described here below.

We started performing several sets of simulations. In all cases, we have imposed fixed boundary conditions on the left side to ensure a zero frequency[9] and free boundary conditions on the right side with different values of the torque f_1 (see the caption of figure 5 for additional details). In some cases (see the red, dark green and blue

[9] The frequency can be afterwards shifted by an arbitrary amount, without altering the physical properties.

lines in figure 5(a)) no thermal bath was used on the left boundary, which automatically implies a vanishing heat flux (while the momentum flux self-adjusts on the basis of both boundary conditions).

According to the theoretical considerations reported in section 2, a meaningful comparison among the different cases can be performed only after choosing a suitable reference frame where the energy flux vanishes, i.e. by replacing ω with the shifted frequency ω_e (see equation (8)). The corresponding curves are reported in panel (b) of figure 5: the seemingly unphysical phenomenon of mutual crossing of the different paths present in panel (a) has disappeared, thus confirming that T and ω_e are proper thermodynamic variables. The final step of this data analysis consists in redrawing the paths in the $(\sigma,\ T)$-plane, where $\sigma = \omega_e^2$. The result is shown in figure 5(c), where the abscissa has been chosen in such a way that all paths have in common the point corresponding to $T_1 = 0.5$ (notice that $\sigma_{\max} = (f_1 - \omega_e)^2$ is a path dependent quantity), while the leftmost value of the abscissa for each path corresponds to the maximum value of T along the path.

The very good data collapse confirms that the thermodynamic behavior of coupled transport in the XY chain is determined by T only. Notice that this result holds also for the purple path in figure 5, which extends to negative values of ω_e: in fact, what matters is ω_e^2, irrespective of the sign of the frequency itself.

From this analysis one understands that the origin of the temperature bump can be traced back to a constant negative derivative of $\mathrm{d}T/\mathrm{d}\sigma$, which in turn follows from the positive sign of the ratio L_{pp}/L_{qq} which is fixed by thermodynamic conditions (see equation (11)).

Moreover, the clean linear dependence of T on σ ($\mathrm{d}T/\mathrm{d}\sigma \approx -0.28$) indicates that, at least in some temperature range[10] equation (11) thus becomes

$$\frac{L_{qq}}{L_{pp}} \equiv D \approx \frac{T}{0.56I}. \tag{15}$$

Here, the (equal to 1) moment of inertia I has been added for dimensional reasons (the ratio L_{qq}/L_{pp} has the dimension of a squared frequency), to stress that 0.56 is a pure adimensional number. We have no arguments to justify its value.

By then making use of equation (14), one can determine the dependence of L_{qq} on T: see the red lines displayed in figure 4. One could obtain L_{qq} from from standard heat-transport simulations in the absence of momentum flux. The implementation of such a direct procedure to chains with small temperature gradient yields the green triangles reported in the same figure 4. The relatively good agreement confirms the correctness of our approach to coupled transport.

Coming back to figure 3, the shape of both temperature and frequency profiles is dictated by the 'material' of the chain of rotors, i.e. by the dependence of the transport coefficients $L_{pp}(T)$ and $L_{qq}(T)$ on the temperature itself. If the external frequency gradient is sufficiently small, one can assume that the momentum conductivity $\rho = L_{pp}/T$ is constant along the chain. In this limit equation (14) implies a linear frequency profile $\omega(y) = \omega_0 + (\omega_1 - \omega_0)y$. By then using the constant slope $\mathrm{d}T/\mathrm{d}\sigma = -c$ obtained from figure 5, one obtains a quadratic temperature profile

$$T(y) = -c[(\omega^2(y) - \omega_0^2) - 2\overline{\omega}(\omega(y) - \omega_0)] + T_0 \tag{16}$$

that represents a parabola with a coefficient of the second order term (openness) $c\,(\omega_1 - \omega_0)^2$ where $c \approx 0.28$. The dashed lines in figure 3 show the constant-conductivity approximation around $y = 0.5$ for the numerical profiles in panels (a) and (b).

5. Coupled transport in the DNLS equation

In this section we discuss coupled transport in the DNLS equation, a more general model, where thermodynamic properties do not only depend on the temperature, but also on the chemical potential. The evolution equation is

$$\mathrm{i}\dot{z}_n = -2|z_n|^2 z_n - z_{n+1} - z_{n-1}, \tag{17}$$

where z_n is a complex variable and $|z_n|^2$ is the local norm. This system is particularly interesting because of its important applications in many domains of physics ranging from waveguide optics, biomolecules and trapped cold gases [39]. The DNLS Hamiltonian has two conserved quantities, the mass/norm density a and the energy density h (for details see [40, 41]). Accordingly, it is a natural candidate for describing coupled transport [18, 37], which can be studied by introducing the Langevin equation [37] (specified for the last lattice site)

$$\mathrm{i}\dot{z}_N = (1 + \mathrm{i}\gamma)[-2|z_N|^2 z_N - z_{N+1} - z_{N-1}] + \mathrm{i}\gamma\mu z_N + \sqrt{\gamma T}\ \eta(t). \tag{18}$$

[10] Preliminary simulations performed at smaller temperatures suggest that the paths in the $(\sigma,\ T)$-plane bends down, while approaching the zero temperature axis.

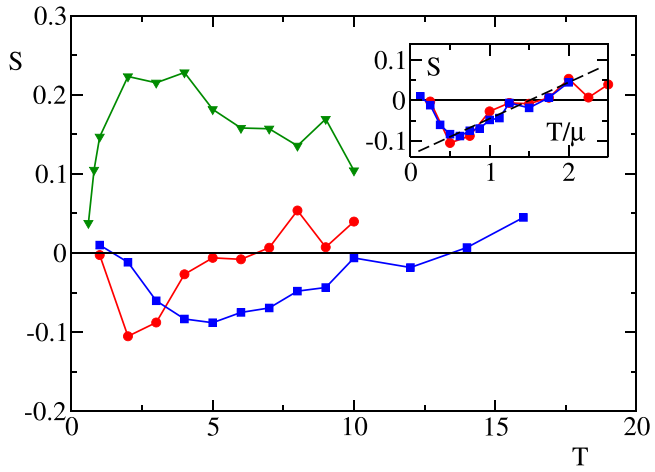

Figure 6. The DNLS Seebeck coefficient S as a function of the temperature T for three different chemical potentials: $\mu = 0$ (green triangles), $\mu = 4$ (red circles) and $\mu = 8$ (blue squares). In the inset: the curves with $\mu = 4$ and $\mu = 8$ in the rescaled temperature representation T/μ. The black dashed curve is a linear approximation of S around $S = 0$ with slope 0.09. Simulations have been performed imposing $\Delta T = 0.1T$ and $\Delta\mu = 0.1$ on DNLS chains with $N = 400$ lattice sites initially in equilibrium at T, μ. The three leftmost points of the curve $\mu = 0$ refer to DNLS with $N = 800$.

Here μ is the chemical potential imposed by the bath and $\eta(t)$ is a complex Gaussian white noise with zero mean and unit variance. In the high-temperature regime transport is normal [18] and fluctuations of conserved fields spread diffusively [42]. However, in the low temperature regime phase slips are rare, with the consequence that phase differences appear as an additional (almost) conserved field, yielding anomalous transport on very long timescales [42].

Unlike the XY model, the two currents associated with the conservation laws are mutually coupled in the DNLS equation. On the other hand, in a recent paper [37] it was argued that in the high mass-density limit (i.e. for large chemical potentials μ) the DNLS dynamics is well approximated by that of a XY chain in equilibrium simulations. However, a precise identification of the parameter region where an accurate mapping is expected has not yet been fully worked out. One of the reasons is the non uniformity of the thermodynamic limit: no matter how long the system is, intermittent bursts always occur possibly invalidating the existence of a precise relationship. It is therefore important to explore the connection between the two models from the point of view of irreversible thermodynamics, comparing for instance the associated Onsager coefficients.

In [37] it was found that in the large mass limit a thermostatted DNLS equation with parameters T and μ is equivalent to the XY model

$$\begin{aligned} \dot{\phi_N} &= p_N, \\ \dot{p}_N &= U\left[\sin(\phi_{N+1} - \phi_N) - \sin(\phi_N - \phi_{N-1})\right] - \gamma'(p_N - \delta\mu) + \sqrt{4\gamma' T}\,\xi(t), \end{aligned} \tag{19}$$

where $\gamma' = U\gamma$. Here we have defined $\mu = (U/2 - 2) + \delta\mu$, which corresponds to describing the DNLS model in a rotating reference frame with frequency $(\mu - \delta\mu) = (U/2 - 2) \gg \delta\mu$. This choice does not limit the generality of the mapping, since any other choice of the reference frame would produce a shift of all the XY phase velocities that can be eliminated by the gauge transformation described in section 2. Finally, by looking at the stochastic term and comparing it with the analogous term in equation (13) one notices a factor 2 difference in the definition of the temperature: this point will be important later on.

From a thermodynamic point of view, the major difference between the rotor model and DNLS equation is that in the former case, the off-diagonal elements $L_{pq} = L_{qp}$ vanish. Therefore, the adimensional Seebeck coefficient

$$S = \frac{1}{T}\frac{L_{pq}}{L_{pp}} \tag{20}$$

is a proper indicator to test the closeness of the two models.

Figure 6 shows the dependence of the Seebeck coefficient in the DNLS model on the temperature for three different values of the chemical potential μ. Upon increasing μ we indeed see that S decreases and crosses the zero axis for some finite temperature. The two curves for $\mu = 4$ and $\mu = 8$ indicate that the zero-Seebeck condition occurs approximately for a temperature that is proportional to μ, $T_c \sim 1.5\mu$ (see the inset). In the neighborhood of T_c the Seebeck coefficient grows almost linearly $S \sim 0.09\ T/\mu$ (see the red dashed line). A consistent equivalence with the XY chain in a broad range of parameter values would require that upon

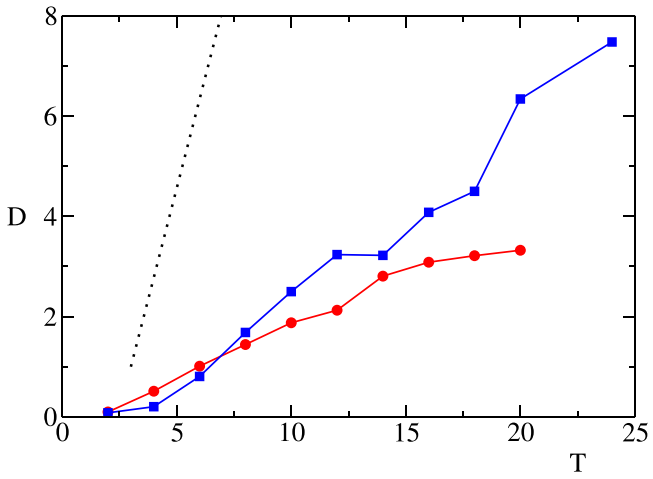

Figure 7. The ratio of the diagonal Onsager coefficients $D = Lqq/Lpp$ for the DNLS equation with average chemical potential $\mu = 4$ (red circles) and $\mu = 8$ (blue squares). The simulation parameters are the same as in figure 6. The black dotted line corresponds to the slope as expected from the study of the rotor model.

increasing μ the slope should decrease. In so far as it stays constant, as our simulations seem to suggest, a quantitative agreement is restricted to a tiny temperature-interval around T_c.

For a complete characterization of the DNLS transport, it is instructive to look also at the diagonal elements of the Onsager matrix and, in particular at the ratio $D = L_{qq}/L_{pp}$. In figure 7 we plot D as a function of the temperature T, multiplied by a factor 2, to take into account the scale difference with the XY model. An approximately linear growth is found that is analogous to the behavior observed in the rotor model. The slope is, however, smaller (see the dotted curve) although it keeps increasing with the value of the chemical potential. Accordingly we can conjecture that upon further increasing μ a better agreement could be found, but more refined simulations are necessary for a more quantitative statement.

6. Discussion and conclusions

In this paper we have provided a detailed analysis of the structure of nonequilibrium steady states in the presence of coupled transport. In both the considered models (XY and DNLS), the relevant variable is an angle and that is the reason why (especially in the XY case) the coupling between angular-momentum and energy currents gives rise to nontrivial phenomena. In generic nonlinear chains, like the Fermi–Pasta–Ulam model or similar [1, 2], particles characterized by different velocities would inevitably fall apart with no mutual interactions; in our set-up the very nature of the angular variables (defined, say, between 0 and 2π) induces a different physical scenario. The XY-dynamics is nevertheless reminiscent of the evolution of nonlinear oscillators in that no coupling is present between heat and angular momentum current (this statement is equivalent to saying that the Seebeck coefficient is identically equal to zero). In spite of its extremely simplified structure, we have shown that this setup can sustain coupled transport whenever a torque is applied to the chain ends. The reason is due to the emergence of a coherent energy flux, which acts as a mediator. It is foreseeable that a deeper understanding will be useful in the problem of nano and mesoscale heat transport. For instance, in the context of Josephson physics it has been recently demonstrated that some form of coherent heat transport may be used for control in special applications [43]. As a coherent contribution is expected to arise in more general physical setups, an important advice can be given for future studies, namely that of singling it out and distinguishing it from the coupling which involves the heat flux.

The DNLS is a model where heat flux is directly coupled with norm flux. However, consistently with a previous claim [37], our numerical simulations show that in the limit of large chemical potential the DNLS equation reduces to the XY rotor model. In particular, we find that the critical line separating positive from negative values of the Seebeck coefficients, extend to large μ-values. This encourages the performance of further studies to put the equivalence on a firmer basis and to possibly use the equivalence as a starting point for a perturbative analysis.

Finally, additional studies of the XY model are welcome both in the region of small temperatures, where the confinement within the energy valley becomes crucial (we are currently working in this direction) and of high-temperatures, where for different reasons a dynamical ergodicity breaking is expected (see e.g. [36]), which strongly modifies transport properties.

Acknowledgments

One of us (AP) wishes to acknowledge S Flach for enlightening discussions about the relationship between the DNLS equation and the rotor model.

References

[1] Lepri S, Livi R and Politi A 2003 *Phys. Rep.* **377** 1
[2] Dhar A 2008 *Adv. Phys.* **57** 457–537
[3] Basile G, Delfini L, Lepri S, Livi R, Olla S and Politi A 2007 *Eur. Phys. J. Spec. Top.* **151** 85–93
[4] Lepri S (ed) 2016 *Thermal Transport in Low dimensions: From Statistical Physics to Nanoscale Heat Transfer* (*Lecture Notes in Physics* vol 921) (Berlin: Springer)
[5] Wang L, Hu B and Li B 2013 *Phys. Rev.* E **88** 052112
[6] Wang L and Wang T 2011 *Europhys. Lett.* **93** 54002
[7] Lepri S, Mejía-Monasterio C and Politi A 2009 *J. Phys. A: Math. Theor.* **42** 025001
[8] Das S G, Dhar A, Saito K, Mendl C B and Spohn H 2014 *Phys. Rev.* E **90** 012124
[9] Lee-Dadswell G 2015 *Phys. Rev.* E **91** 032102
[10] Spohn H 2014 *J. Stat. Phys.* **154** 1191–227
[11] Das S, Dhar A and Narayan O 2014 *J. Stat. Phys.* **154** 204–13
[12] Liu S, Hänggi P, Li N, Ren J and Li B 2014 *Phys. Rev. Lett.* **112** 040601
[13] Mejía-Monasterio C, Larralde H and Leyvraz F 2001 *Phys. Rev. Lett.* **86** 5417–20
[14] Casati G, Wang L and Prosen T 2009 *J. Stat. Mech.* L03004
[15] Benenti G, Casati G and Mejía-Monasterio C 2014 *New J. Phys.* **16** 015014
[16] Gillan M and Holloway R 1985 *J. Phys. C: Solid State Phys.* **18** 5705–20
[17] Basko D 2011 *Ann. Phys., NY* **326** 1577–655
[18] Iubini S, Lepri S and Politi A 2012 *Phys. Rev.* E **86** 011108
[19] De Roeck W and Huveneers F 2015 *Commun. Pure Appl. Math.* **68** 1532–68
[20] Borlenghi S, Iubini S, Lepri S, Chico J, Bergqvist L, Delin A and Fransson J 2015 *Phys. Rev.* E **92** 012116
[21] Escande D, Kantz H, Livi R and Ruffo S 1994 *J. Stat. Phys.* **76** 605–26
[22] Giardiná C, Livi R, Politi A and Vassalli M 2000 *Phys. Rev. Lett.* **84** 2144–7
[23] Gendelman O V and Savin A V 2000 *Phys. Rev. Lett.* **84** 2381–4
[24] Yang L and Hu B 2005 *Phys. Rev. Lett.* **94** 219404
[25] Li Y, Liu S, Li N, Hänggi P and Li B 2015 *New J. Phys.* **17** 043064
[26] Mendl C B and Spohn H 2013 *Phys. Rev. Lett.* **111** 230601
[27] Das S G and Dhar A 2014 arXiv:1411.5247
[28] Flach S, Miroshnichenko A and Fistul M 2003 *Chaos* **13** 596–609
[29] Eleftheriou M, Lepri S, Livi R and Piazza F 2005 *Physica* D **204** 230–9
[30] Cuneo N and Eckmann J P 2016 *Commun. Math. Phys.* **345** 185–221
[31] Gendelman O and Savin A 2010 *Phys. Rev.* E **81** 020103
[32] Iacobucci A, Legoll F, Olla S and Stoltz G 2011 *Phys. Rev.* E **84** 061108
[33] Iubini S, Lepri S, Livi R and Politi A 2014 *Phys. Rev. Lett.* **112** 134101
[34] Ke P and Zheng Z G 2014 *Front. Phys.* **9** 511–8
[35] Delfini L, Lepri S and Livi R 2005 *J. Stat. Mech.* P05006
[36] Pino M, Ioffe L B and Altshuler B L 2016 *Proc. Natl Acad. Sci.* **113** 536–41
[37] Iubini S, Lepri S, Livi R and Politi A 2013 *J. Stat. Mech.* P08017
[38] Spohn H 2014 arXiv:1411.3907
[39] Kevrekidis P G 2009 *The Discrete Nonlinear Schrödinger Equation* (Berlin: Springer)
[40] Rasmussen K, Cretegny T, Kevrekidis P G and Grønbech-Jensen N 2000 *Phys. Rev. Lett.* **84** 3740–3
[41] Iubini S, Franzosi R, Livi R, Oppo G and Politi A 2013 *New J. Phys.* **15** 023032
[42] Mendl C B and Spohn H 2015 *J. Stat. Mech.* P08028
[43] Giazotto F and Martínez-Pérez M J 2012 *Nature* **492** 401–5